Applied Catalysis B: Environmental 111–112 (2012) 141–149

Contents lists available at SciVerse ScienceDirect

Applied Catalysis B: Environmental

journal homepage: www.elsevier.com/locate/apcatb

Effect of Ce and La on the structure and activity of MnO_x catalyst in catalytic combustion of chlorobenzene

Yu Dai, Xingyi Wang*, Qiguang Dai, Dao Li

Laboratory for Advanced Materials, Research Institute of Industrial Catalysis, East China University of Science and Technology, P.O. 396, 130 Meilonglu, Shanghai 200237, China

ARTICLE INFO

Article history:
Received 25 April 2011
Received in revised form 26 August 2011
Accepted 23 September 2011
Available online 29 September 2011

Keywords:
Chlorobenzene
Catalytic combustion
Cl adsorption
Thermal stability
$MnCeO_x$ solid solution

ABSTRACT

Mn-based oxide-mixed catalysts modified with Ce and La, which were prepared by complexation method, were tested in the catalytic combustion of chlorobenzene (CB) as a model of chlorinated aromatics. The characterization by XRD, XPS, TPR and Raman shows that the addition of Ce makes a large portion of Mn species enter CeO_2 fluorite, leading to the formation of $MnCeO_x$ solid solution. The structure to be composed of MnO_x and $MnCeO_x$ solid solution is highly active for CB oxidation due to the presence of a large amount of active oxygen species. The addition of La can promote the thermal stability of $MnCeO_x$ solid solution during calcination up to 750 °C, and accordingly the catalyst presents high activity. The study on reaction kinetics shows zero order on CB concentration in the presence of the catalysts except for MnCe-550, indicating that adsorption strength of Cl species produced during the reaction is critical to CB combustion because the adsorbed Cl species can decrease the reducibility of Mn species, thus the mobility of oxygen. Nevertheless, high activity, good selectivity and desired stability were observed over MnCeLa catalysts at 350 °C.

1. Introduction

Aryl chlorides are hazardous pollutants that are considered among the most harmful organic contaminants due to their acute toxicity and strong bioaccumulation potential [1], and therefore, the safe disposal of aryl chloride pollutants has acquired great importance with the ever increasing concern for environmental protection [2]. Among various available techniques, catalytic combustion is an interesting. This technology can be efficiently performed within the temperature range from 250 to 550 °C to convert so dilute the pollutants that otherwise thermal combustion with consumption of fuel is necessary. Of the studies of the catalysts used in the catalytic combustion of aryl chlorides, most have been reported on the three types of catalysts based on noble metals, transition metals and zeolites [3–5]. Among the catalysts used for catalytic combustion of aryl chlorides, transitional metal oxides, i.e., V-based oxide catalysts, especially V_2O_5/TiO_2 catalysts, which are widely used in combustion of chlorobenzene (CB), present high activity and stability [6–8].

As known, manganese oxides are considered as environmentally friendly materials [9]. Many efforts were paid for exploring the application of manganese oxides in catalytic combustion of volatile organic exhaust. It has been verified that manganese oxides are highly active in the oxidation of hydrocarbons, due to their high efficiency in the reaction/oxidation cycles [10–13]. Moreover, the redox capabilities are strongly enhanced when combined with other elements [14]. Although pure manganese oxides will deactivate during the oxidation of chlorinated hydrocarbon, their resistance to the attack by Cl species can be really promoted by the addition of other elements [8]. In our previous work, Mn-based oxide catalysts of either the supported or the unsupported, particularly $MnCeO_x$ oxide-mixed catalysts prepared by complexation method, have high activity in catalytic combustion of CB [15–17]. Activity and stability of $MnCeO_x$ oxide-mixed catalysts are found to be related to the particle size of $MnCeO_x$ solid solution which has a fluorite-like structure with a large amount of surface oxygen adequately supplied to the oxidation for the final removal of the formed chloride species. However, the main challenge to these binary oxides is the easy sintering at high temperature so that small particles aggregate and solid solutions collapse due to phase segregation.

As additive or support, La_2O_3 has been widely investigated due to its thermal stability and diverse crystalline phases. La_2O_3 can interact with transitional metal oxides to form perovskite-structured oxides, ABO_3, of which $LaMnO_3$, modified by doping metal ions, has high activity and selectivity in the oxidation of methane [18,19]. Moreover, La can promote the thermal stability of the catalyst through formation of solid solution with other oxides, such as Ce–La–O [20,21], Al–La–O [22]. Here, the incorporation of La and Ce into MnO_x may offer an opportunity to prepare novel catalysts with high performance for the catalytic oxidation of chlorobenzene. In the present work, Mn-based catalysts doped

* Corresponding author. Tel.: +86 21 64253372; fax: +86 21 64253372.
E-mail address: wangxy@ecust.edu.cn (X. Wang).

0926-3373/$ – see front matter © 2011 Elsevier B.V. All rights reserved.
doi:10.1016/j.apcatb.2011.09.028

with La and Ce were prepared by complexation method, resulting in the significant improvement of catalytic activity and stability in CB combustion as well as resistance to particle sintering.

2. Experimental

2.1. Catalysts preparation

Mn-based catalysts doped with La and Ce were prepared by complextion method: an aqueous solution containing $Mn(NO_3)_2$, $Ce(NO_3)_3{\cdot}6H_2O$ (SCRC, 99.0%), $La(NO_3)_3{\cdot}6H_2O$ (SCRC, 99.0%) (Mn:Ce:La = 8:1:1), citric acid (SCRC, 99.0%) (citric acid:(Mn/1.5 + Ce+ La) = 0.3) was gradually heated to 80 °C and kept at this temperature for 7 h while stirring, so that a yellowish sticky suspension was finally formed. The suspension was then dried at 110 °C for 12 h, followed by calcination at predetermined temperature for 5 h in air. The synthesized catalysts are denoted as MnCeLa-*T*, where *T* represents the calcination temperature. The same method was employed in preparation of catalysts MnCe-*T* (Mn:Ce = 8:2), MnO_x-*T* and MnLa-*T* (Mn:La = 8/2), which were used as reference samples, with which catalysts MnCeLa-*T* were compared.

2.2. Catalyst characterization

The powder X-ray diffraction patterns (XRD) of the samples were recorded on a Rigaku D/Max-rC powder diffractometer using Cu Kα radiation (40 kV and 100 mA). The diffractograms were recorded as 2θ ranging from 10° to 80° with step size of 0.01° and the step time of 10 s. The nitrogen adsorption and desorption isotherms were measured at 77 K on an ASAP 2400 system operated in static measurement mode. The samples were outgassed at 160 °C for 4 h before the measurement. The specific surface area was calculated using the BET model. The XPS measurements were made on a VG ESCALAB MK II spectrometer by using Mg Kα (1253.6 eV) radiation as the excitation source. Charge of samples was corrected by setting the binding energy of adventitious carbon (C1s) at 284.6 eV. The powder samples, in the form of the pressed self-supporting disks, were loaded into a sub-chamber, which was vacuumed for 4 h before the measurement at 298 K. H_2-temperature programming reduction (H_2-TPR) was investigated by heating catalysts (50 mg) in H_2 (5 vol.%)/Ar flow (30 ml min^{-1}) at a heating rate of 10 °C min^{-1} from 50 to 750 °C. The hydrogen consumption was monitored by thermo-conductivity detector. Before the H_2-TPR analysis, the samples were heated for 60 min in Ar flow at 300 °C. Raman spectra were recorded on Via Reflex Laser Raman instrument, equipped with a CCD (charge coupled device) detector. The excitation source was the 514.5 nm line of Ar ion laser. The laser power was set at 3 mW. All data or results obtained from characterization test are repeated basically three times.

2.3. Catalytic activity measurement

Catalytic combustion reaction was carried out at atmospheric pressure in a continuous flow micro-reactor made of a quartz tube with inner diameter of 4 mm. 200 mg catalyst as the reaction bed was packed. The feeding flow rate to the reactor was set at 50 cm^3 min^{-1} and the gas hourly space velocity (GHSV) was maintained at 15,000 h^{-1}. Feed stream to the reactor was prepared by delivering liquid CB with a syringe pump into dry air, which was metered by a mass flow controller controlling CB concentration in the feed stream at 1000 ppm. The injection part is electrically heated to ensure complete evaporation of CB. The temperature of the reactor was measured with a thermocouple located just at the exit of the microreactor. The effluent gases were analysed on-line at a given temperature by using two gas chromatographs (FULI 9790), one equipped with FID for the quantitative analysis of the organic chlorinated reactant, and the other one with TCD for CO and CO_2. Combining the analyses by mass spectrometry (HIDEN ANALYTIC HPR20), the effluents can be identified. The conversion datum on the given temperature is the average value of five sampling analyses. The concentrations of Cl_2 and HCl were analysed by the effluent stream bubbling through a 0.0125 N NaOH solution, and chlorine concentration was then determined by the titration with ferrous ammonium sulphate (FAS) using N,N-diethyl-p-phenylenediamine (DPD) as indicator [23]. Here, it should be noted that the total error caused in these processes may be within ±5%. The concentration of chloride ions in the bubbled solution was determined by using a chloride ion selective electrode [24].

3. Results and discussion

3.1. Characterization of catalysts

3.1.1. XRD

Wide angle XRD patterns of catalysts are shown in Fig. 1. For pure MnO_x samples calcined at different temperatures, there appear five intense and sharp peaks at 32.9°, 38.13°, 49.56°, 55.17° and 65.77°, the indices of incipient α-Mn_2O_3 crystallization in the form of bixbyite (JCPDS #24-0508) [25]. And pure CeO_2 in the form of cerianite with a fluorite-like structure exhibits diffraction peaks at 28.7°, 33.3°, 47.5°, 56.5° and 59.2° (JCPDS #43-1002). For MnCe-550 sample, the reflection from MnO_x or CeO_2 can not be observed on XRD pattern, indicating that the dispersion of both Mn and Ce species greatly increases. By raising calcination temperature of MnCe catalyst up to 650 °C, the diffraction peaks from α-Mn_2O_3 become significantly strong. Slight asymmetry shape of reflection with lower intensity from cerianite confirms the weakening degree of the crystallinity of cerianite in MnCe-650 sample. The Bragg angle of cerianite shifting slightly to the high value indicates that Mn^{3+} or Mn^{4+} species enters the fluorite-like lattice, leading to the information of $MnCeO_x$ solid solution [26]. For MnCe-750 sample, the reflections from cerianite become much stronger, indicating that CeO_2 crystal particles become larger (see Table 1). At the same time, the intensity of reflections from α-Mn_2O_3 greatly increases, implying that Mn species dissociate from the $MnCeO_x$ solid solution during calcinations at high temperature. For MnLa-550 sample, the reflections appear only from α-Mn_2O_3. These reflections become stronger for MnLa-650 and MnLa-750 samples, as the result of aggregation of the corresponding crystalline particles. Additionally there appear weak reflections from $LaMnO_3$ at 40.12°, 46.71° and 58.07° (JCPDS #54-1275).

MnCeLa samples calcined at different temperatures present lower intensity of reflections from cerianite. Moreover, the shift of Bragg angle of ⟨1 1 1⟩ from 28.6° of pure CeO_2 to 29.1° indicates the formation of $MnCeO_x$ solid solution. For the MnCeLa catalysts calcined at 650 and 750 °C, the slight increase in intensity of reflections from cerianite indicates the growth of cerianite crystal particles during calcinations (Table 1). Meanwhile, there appear diffraction peaks of α-Mn_2O_3. Ye and Xu [27] reported that the amount of Mn species entering the fluorite-like lattice is limited to 70%. It is reasonable to assume that MnCeLa catalysts contain a significant amount of α-Mn_2O_3.

As known, the possibility of the formation of $LaCeO_x$ solid solutions can exist under the conditions as described in this work [22,28]. If the La^{3+} ions are incorporated into the fluorite lattice, the value of lattice parameter should increase [20,21]. However, the lattice parameters of cerianite for MnCeLa catalysts calcined at different temperatures fall within the range of 5.32–5.38 Å (Table 1.). Compared with the value (5.35–5.39 Å) obtained from

Table 1
The properties of MnCe and MnCeLa catalysts calcined at different temperatures.

Catalyst	Surface area (m^2/g)	$d_{222}(MnO_x)$ (Å)	D_{MnOx} /nm[a]	d_{111} (CeO_2) (Å)	D_{CeO_2} (nm[b])	Phase
CeO_2-550	9			3.12	13.9	Cerianite (CeO_2)
Mn550	9	2.72	26.2			Bixbyite (Mn_2O_3)
Mn650	8	2.72	27.1			Bixbyite (Mn_2O_3)
Mn750	8	2.72	27.9			Bixbyite (Mn_2O_3)
MnCe-550	65	2.72	20.0	3.09	NT	Cerianite (Mn–Ce–O)[b]
MnCe-650	38	2.72	24.6	3.12	10.4	Cerianite(CeO_2), Bixbyite (Mn_2O_3)
MnCe-750	21	2.72	26.0	3.12	11.5	Cerianite (CeO_2), Bixbyite (Mn_2O_3)
MnLa-650	13	2.72	17.5			Bixbyite (Mn_2O_3), Perovskite ($LaMnO_3$)
MnLa-750	10	2.72	15.0			Bixbyite (Mn_2O_3), Perovskite ($LaMnO_3$)
MnCeLa-550	97	2.71	19.1	3.07	NT	Cerianite (Mn–Ce–O)[c]
MnCeLa-650	65	2.71	20.8	3.09	6.5	Cerianite (Mn–Ce–O)[c], Bixbyite (Mn_2O_3)
MnCeLa-750	54	2.71	22.2	3.11	7.8	Cerianite (Mn–Ce–O)[c] Bixbyite (Mn_2O_3) Perovskite ($LaMnO_3$)

[a] The value estimated by the Scherrer equation, applied to the ⟨2 2 2⟩ reflection of the bixbyite(Mn_2O_3).
[b] The value estimated by the Scherrer equation, applied to the ⟨1 1 1⟩ reflection of the cerianite;[c] Solid solution with fluorite-like structure. NT, not detected.

$MnCeO_x$ solid solutions [16], it can be suggested that $LaCeO_x$ solid solutions exist in a small fraction of the total amount. Additionally, the reflections from La species, such as La_2O_3 and $LaMnO_3$, cannot be observed, probably due to a high dispersion of La species either into or between the matrix of Mn species or $MnCeO_x$ solid solutions. But, for MnCeLa-750 catalyst, there appear weak reflections from $LaMnO_3$.

3.1.2. XPS

Characterization of chemical species located in the region near the catalyst surface was carried out by XPS and the results are summarized in Table 2. The O1s spectra (shown in Fig. 2) exhibit two features. The peak at lower binding energy, 529.4–530.0 eV, corresponds to lattice oxygen (O^{2-}), whereas the one at 531.3–531.8 eV corresponds to Ols states assigned to the surface-adsorbed oxygen such as O_2^{2-} or O^- taking the forms of hydroxyl OH^- and carbonate CO_3^{2-} species (all fall in the range of 531–532 eV) as well as the adsorbed molecular water (above 533.0 eV) [29–34]. For pure MnO_x sample, the peak at 529.8 eV is assigned to lattice oxygen. Incorporation of Ce makes O1s level shift to 529.5 eV, consistent with that of the lattice oxygen in $MnCeO_x$ solid solution, indicating that most Mn species on the surface take the form of $MnCeO_x$ solid solution [28]. However, for MnCe-650 sample, two binding energies of lattice oxygen of 529.7 and 528.0 eV are observed. The former can be the lattice oxygen in MnO_x, and the latter, the lattice oxygen in CeO_2 [16]. This indicates that main part of Mn species is not included in $MnCeO_x$ solid solution. Additionally, the increase in the amount of Ce on the surface of MnCe-650 and MnCe-750 is observed by XPS (Table 2).

The binding energies of Mn $2p_{3/2}$ (Fig. 2) are very similar to those reported in the literature i.e., Mn species with Mn 2p levels of 639.9, 641.0 and 642.3 eV on the surface of catalysts containing Mn can be ascribed to Mn^{2+}, Mn^{3+} and Mn^{4+} ions [29,32,35,19]. Since the differences between the binding energy values of Mn^{3+} and Mn^{4+} ions are small, a peak synthesis procedure, which includes four components – Mn^{2+}, Mn^{3+}, Mn^{4+} and a satellite [29,32,35,19] was applied. The fitted XPS spectra of Mn 2p are shown in Fig. 2. For MnO_x-550, MnCe-650 and MnCe-750, there exists a significant amount of Mn^{2+} species. Mn^{2+} species in MnO_x-550 may be ascribed to the existence of precursor, while the ones in MnCe-650 and MnCe-750, to the removal of oxygen during the calcinations at 650 or 750 °C. The general transition of MnO_x at elevated temperatures due to the loss of lattice oxygen has been demonstrated as in the following scheme [17].

$$Mn_2O_3 \xrightarrow{90\,^\circ C} Mn_3O_4 \xrightarrow{1700\,^\circ C} MnO$$

Generation of bulk Mn_3O_4 occurs only when calcination temperature is higher than 900 °C. Therefore, we suggest that the oxygen releases from decomposition of MnO_x is promoted in the presence of Ce species.

With the addition of La, raising temperature of calcinations only results in the formation of very small amount of Mn^{2+} species, while Mn^{4+}/Mn^{3+} ratio keeps 1.1 (Table 2). From O1s level at

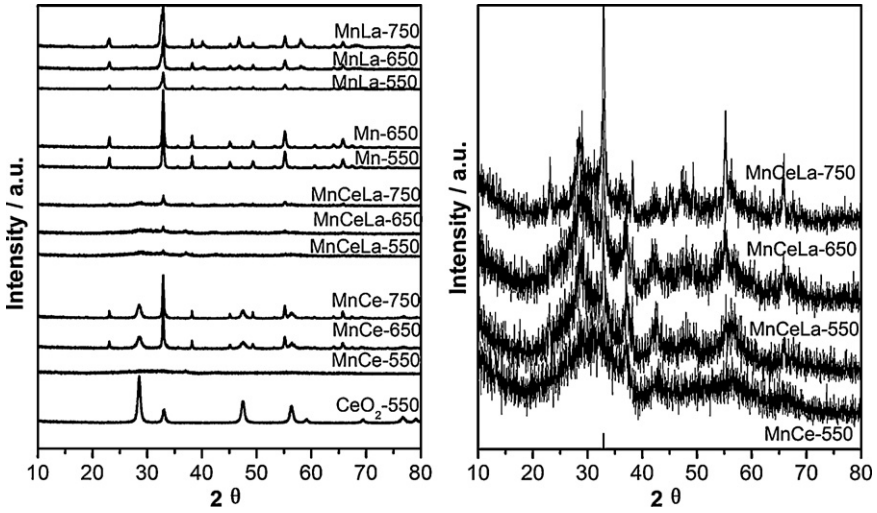

Fig. 1. XRD patterns of MnCe and MnCeLa catalysts calcined at different temperature.

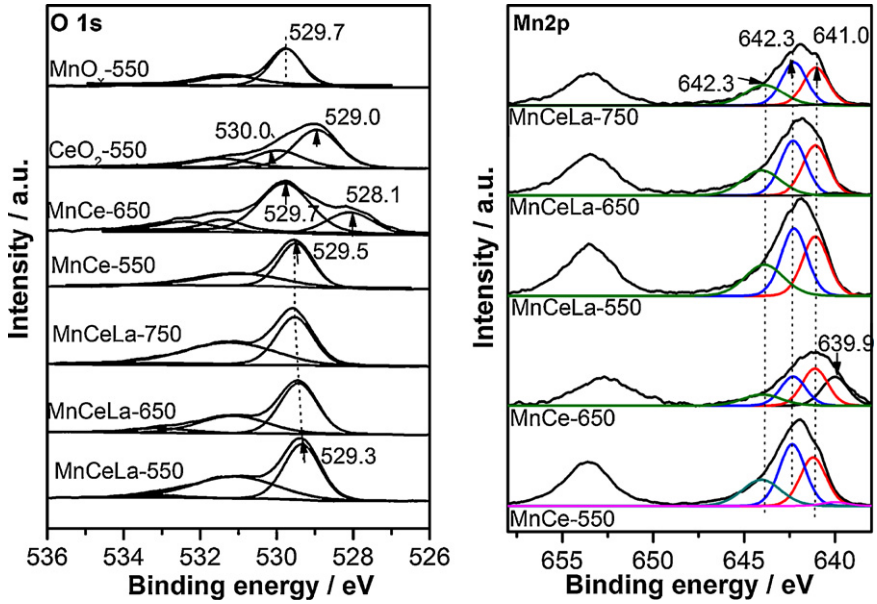

Fig. 2. XPS spectra of O1s and Mn 2p of MnCe and MnCeLa catalysts calcined at different temperature.

529.3–529.4 eV (Fig. 2), it can be deduced that oxygen species is mainly composed of the lattice oxygen in $MnCeO_x$ solid solution. The distribution of elements near surface maintains constant for the samples calcined at different temperatures. These results indicate that the stability of $MnCeO_x$ is promoted by La.

3.1.3. TPR

The results of TPR analyses for catalysts are shown in Fig. 3. Two peaks on TPR profiles result from the reduction of Mn ions belonging to different structures/phases. H_2-TPR profile of pure MnO_x shows two overlapped strong reduction peaks at 374 and 475 °C, respectively. Assuming that MnO is the final reduction state [36] from various Mn species in the initial state of MnO_x, it is reasonable to propose that the peak at low temperature could be assigned to the reduction of MnO_2/Mn_2O_3 to Mn_3O_4, and the peak at high temperature corresponds to the reduction of Mn_3O_4 to MnO [36–38]. As for MnO_x-650, two-step reduction shifts the temperatures to 414 and 519 °C, respectively. It should be noted that the addition of La promotes the reduction of Mn, and the reduction peaks of MnLa-650 appear at 391 and 470 °C, probably due to either the increase in dispersion of Mn species or the formation of $LaMnO_3$ [19]. Moreover, greater H_2 consumption in the second step than that in the first step indicates that the amount of Mn^{3+} is greater than that of Mn^{4+}, a result consistent with XRD that MnO_x-650 and MnLa-650 mainly present α-Mn_2O_3 phase.

Within the range of experimental temperature, the reduction of pure CeO_2 occurs at 526 °C, associated with the reduction of surface Ce^{4+} ions [39], consuming much less H_2 as compared with the reduction features of pure MnO_x. With the addition of Mn into CeO_2, the reduction temperatures of MnCe catalysts systematically shift to lower value. The reduction of Mn species in MnCe-550 occurs at 326 °C in the first step, where H_2 consumption was almost the same as in the second step at 414 °C. Compared with the effect of La, the reduction of Mn species is promoted much more greatly

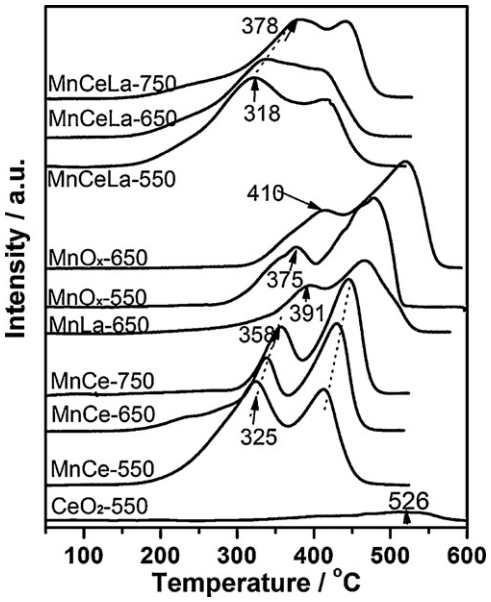

Fig. 3. H_2-TPR of MnCe and MnCeLa catalysts calcined at different temperature.

Table 2
XPS results of MnCe and MnCeLa catalysts calcined at different temperatures.

Catalyst	Mn (at.%)	Ce (at.%)	La (at.%)	Mn (at.%)					O (at.%)		
				Mn^{2+}	Mn^{4+}	Mn^{3+}	Shake	Mn^{4+}/Mn^{3+}	O_{latt}	O_{sur}	O_{ads}
MnO_x	31.1			3.3	8.8	12.8	6.1	0.7	45.6	20.1	3.3
MnCe-550	31.9	3.5	–	0.8	12.9	10.9	8.1	1.2	43.4	14.0	2.0
MnCe-650	19.1	15.0	–	5.0	4.9	6.3	2.9	0.8	43.1	11.7	2.3
MnLa-650	22.6		8.1	NT	9.1	7.5	6.0	1.2	43.6	20.9	4.8
MnCeLa-550	29.1	2.0	4.0	NT	11.3	10.0	7.8	1.1	39.8	18.1	3.8
MnCeLa-650	29.9	1.6	4.3	0.6	11.3	10.3	7.7	1.1	45.1	10.6	1.6
MnCeLa-750	25.7	2.0	4.2	0.3	9.7	8.5	7.1	1.1	47.3	9.5	1.2

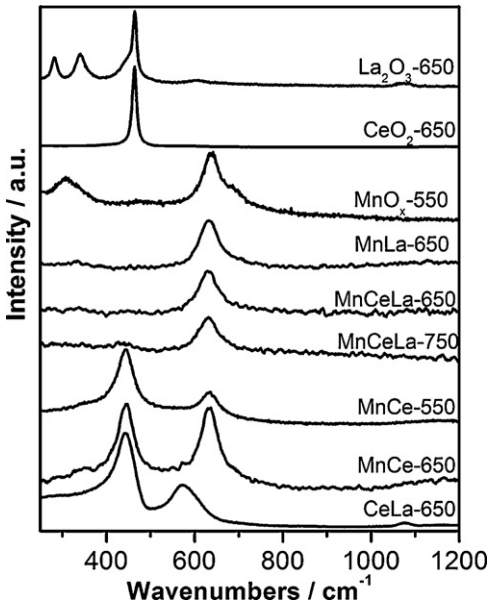

Fig. 4. Raman spectra of MnCe and MnCeLa catalysts calcined at different temperature.

by Ce. This is probable that the reduction of Mn^{4+} occurs through oxygen transfer from MnO_2 to CeO_2. The structure of $MnCeO_x$ solid solution in MnCe-550 favors for the increases in mobility of oxygen species and thus facilitates the reduction of manganese oxide. With the addition of Ce and La into MnO_x, the reduction temperatures of MnCeLa-550 catalyst systematically shift to lower values, and thus two broad overlapped reduction peaks appear around 319 and 412 °C. On the left side of the low temperature peak, it can be observed that the shoulder peak appears around 223 °C, which can be related to the presence of the "isolated" Mn^{4+} ions that "embedded" into the surface defective positions of the ceria lattice. In other words, Mn species on the interface between MnO_x and $MnCeO_x$ can be reduced easily. Furthermore, H_2 consumption in the first step is more than that in the second step, suggesting that more Mn^{4+} ions exist.

Calcination at higher temperature shifts the reduction of samples to high temperature. The first step of reduction for MnCe-650 and MnCe-750 samples occurs at 339 and 356 °C respectively. H_2 consumption decreases significantly, as compared with that in the second step of reduction, indicating that a considerable number of Mn^{3+} ions are reduced in the second step. However, for MnCeLa-650 and MnCeLa-750 samples, H_2 consumption in the first step of reduction is comparable to that in the second step, although reduction temperatures rise to 338 and 373 °C. This phenomenon may be explained by the fact that the ratio of Mn^{4+}/Mn^{3+} changes only slightly (Table 2), and the structure of Mn species is modified to a small extent during calcinations at 650 or 750 °C. The increase in reduction temperature should result from the aggregation of oxide particles at high temperature.

3.1.4. Raman

The possible structure of catalysts was investigated by Raman spectroscopy technique. It can be seen in Fig. 4 that for pure MnO_x catalyst, the peak appearing at 638 cm^{-1} can be attributed to a Mn–O–Mn stretching mode ($\nu_{Mn-O-Mn}$) in Mn_2O_3. This vibration changes slightly because of the addition of La. However, in the case of MnCe-550, the intensity of $\nu_{Mn-O-Mn}$ band with poor symmetry at 638 cm^{-1} becomes much weaker, indicating that Mn species can highly disperse into cerianite and exist in the form of highly asymmetric structure, such as "Mn–O–Mn–O–Ce". At the same time, Raman mode (F2g) of fluorite-like structure [40,41] at 460 cm^{-1} was observed. But this band in pure CeO_2 catalyst appears at 466 cm^{-1}. As known, fluorite-structure is a cubic structure (fcc), in which cations are located on the corners and in the face centres while oxygen atoms are located at the tetrahedral sites. The Raman spectra of ν_{F2g} band are dominated by oxygen lattice vibrations and are sensitive to crystalline symmetry [42]. The shift of ν_{F2g} band by 6 cm^{-1} indicates that the interaction between Mn and Ce should deform the fluorite-like structure and result in the formation of the oxygen vacancies in the CeO_2 lattice [43]. Moreover, the intensity of ν_{F2g} band is strong. It means that well symmetrical peak about Ce species exists, probably as the result of the structure of Mn–O–Ce–O–Mn. For MnCe-650 and MnCe-750, however, the $\nu_{Mn-O-Mn}$ band becomes strong and symmetric, due to the formation of Mn_2O_3. It is interesting to find that the ν_{F2g} band actually disappears for MnCeLa catalysts calcined at various temperatures. This phenomenon implies that Ce–O is highly asymmetric, so that the ν_{F2g} band as a result of the oxygen lattice vibrations becomes dispersive. This asymmetry is probably due to the structure of Mn–O–Ce–O–La.

As known, $CeLaO_x$ solid solution can keep thermally stable up to 800 °C [28]. In this work, XRD result indicates that the main structure of CeLa-750 is of $CeLaO_x$ solid solution. However, decomposition of $MnCeO_x$ solid solution occurs at 650 °C. These results suggest that La–O–Ce bonds are much more stable than Mn–O–Ce bonds. Theoretically, the atomic orbits of La and Ce are of similar feature, and thus it is difficult to rupture La–O–Ce bonds. But the atomic orbit of Mn is very different from that of Ce, and O atoms in $MnCeO_x$ are located in a perturbed chemical surrounding. As the result of it, O atoms become highly mobile during heating, so that MnO_x species can be decomposed into Mn_3O_4 through the removal of oxygen (Mn^{2+} as seen in XPS spectra of MnCe-650 sample). Therefore, improvement of thermal stability of MnCeLa catalysts is probably the result of formation of La–O–Ce–O–Mn.

3.2. Activity of catalysts

Mn-based catalysts under study exhibit high activity in the combustion in the stream containing 1000 ppm CB and 10% O_2 at 350 °C at space velocity of 15,000 h^{-1} (Fig. 5). Over MnO_x-550 catalyst, the complete conversion of CB occurs at 419 °C, while conversion reaches 99% at 549 °C for MnO_x-750. A gradual sintering of α-Mn_2O_3 grains at elevated temperatures may lead to a drastic deactivation of pure MnO_x catalyst [44]. By the addition of La, the activity of both Mn-650 and Mn-750 catalysts is promoted and the conversion curves shift to much lower temperature. This result can be related to the improvement of thermal stability of MnO_x and the formation of $LaMnO_3$. Machocki [19] reported that the activity of $LaMnO_3$ catalysts in the methane combustion was related to the concentration of surface active oxygen. Considering that the mobility of oxygen on MnLa is higher than that on MnO_x (see Section 3.1.3 TPR), it can be deduced that active oxygen may be critical to CB conversion on Mn based catalysts doped with La.

MnCe-550 and MnCeLa-550 appear to be superior for CB catalytic combustion. Conversion of CB reaches 99.0% when reaction proceeds at about 245 and 220 °C, respectively (Fig. 5A); temperatures are much lower than that on MnO_x-550 or MnLa-550, and those on MnO_x/TiO_2–Al_2O_3, MnO_x/TiO_2 [45,46]. As known by the previous reports [16,17,47], the oxygen mobility of MnO_x catalyst was greatly promoted by the incorporation of Ce. In the removal of oxygen, the reconstruction of Mn species will occur. Han reported that a reversible phase-transformation from α-Mn_2O_3 to a Mn_3O_4-like species was observed by Real-time in situ Raman spectroscopy [43]. For catalysts MnCe-550 and MnCeLa-550, the mobility of oxygen species caused through the reconstruction of Mn species

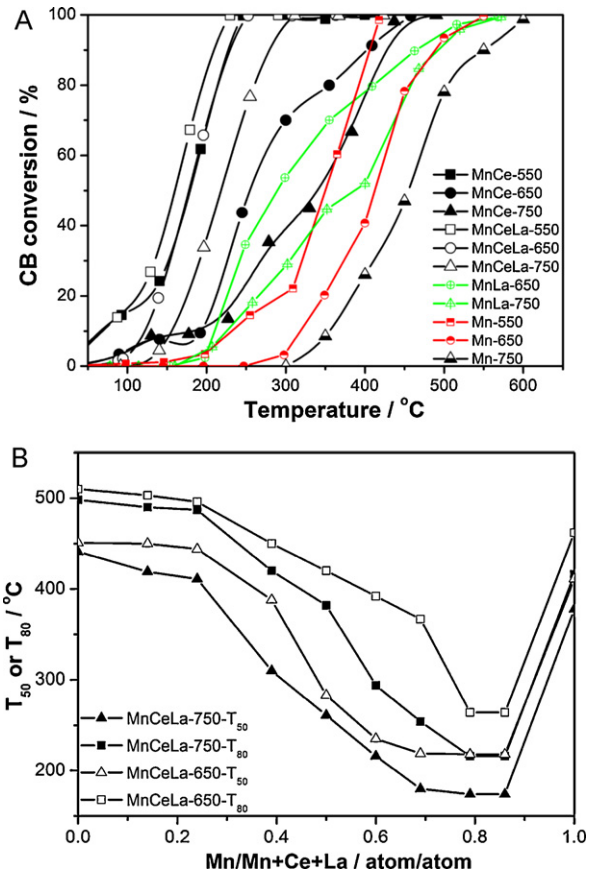

Fig. 5. The activity of MnCe and MnCeLa catalysts for CB catalytic combustion, (A) conversion of CB; (B) $T_{50\%}$ and $T_{80\%}$; gas composition: 1000 ppm CB, 10% O_2, N_2 balance; GHSV = 15,000 h^{-1}.

should be promoted greatly by oxygen vacancies in $MnCeO_x$ solid solution.

For MnCe-650 and MnCe-750 catalysts, the activity drops greatly. The complete combustion of CB occurs at 475 and 500 °C. This is explained by two factors: the decrease in mobility of oxygen species due to the decomposition of $MnCeO_x$ solid solution and enrichment of Ce in a form of CeO_2 on the surface. As known, CeO_2 is susceptible to the strong adsorption of Cl species [48]. The removal of Cl species is a slow process [48], and thus the reaction becomes retarded. The addition of La promotes not only the thermal stability of $MnCeO_x$ solid solution but also Mn species dispersion, so as to maintain the high activity of MnCeLa. Complete conversion over MnCeLa-650 and MnCeLa-750 appears at 220 and 300 °C, respectively.

In order to investigate the effect of $MnCeO_x$ solid solution, catalysts MnCeLa with various Mn/Mn + Ce + La ratios were prepared through calcination at 650 and 750 °C, and activities were thereafter evaluated. The ratio limit of Mn/Mn + Ce for Mn species entering the fluorite lattice is known as 0.60–0.75. When the amount of Mn is decreased below 0.6, almost all of Mn species may exist in the form of $MnCeO_x$ solid solution [49]. In this context, catalysts with the Mn/Mn + Ce + La ratio less than 0.60 (corresponding to Mn/Mn + Ce of 0.75) are suitable to be employed in investigation of the activity of $MnCeO_x$ solid solution for CB combustion. The experimental results in Fig. 5B indicate that T_{50} and T_{80} (where 50% and 80% conversions are reached) increase gradually with the decrease in the Mn/Mn + Ce + La ratio from 0.6 to 0. The change in calcination temperature from 650 to 750 °C does not affect this tendency, although calcination at 750 °C decreases the activity of catalysts of MnCeLa, due to the decrease in surface area. This phenomenon indicates that

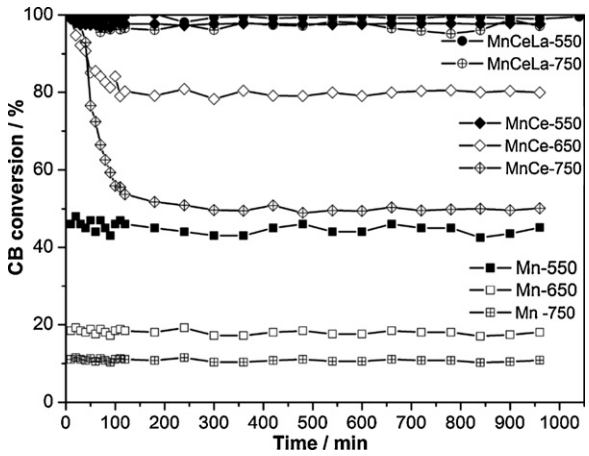

Fig. 6. The stability tests of catalysts calcined at different temperature; gas composition: 1000 ppm CB, 10% O_2, N_2 balance; reaction temperature: 350 °C; GHSV = 15,000 h^{-1}.

$MnCeO_x$ solid solution alone cannot afford the highest activity, but it owns to the synergistic effect between MnO_x and $MnCeO_x$ solid solution during the combustion of CB. In other words, the interface of MnO_x and $MnCeO_x$ solid solution provides high activity for the combustion of CB.

3.3. Analyses of products

Within the performance limit of TCD and FID themselves, all catalysts under study have more than 99.5% selectivity to carbon oxides (more than 98% CO_2 and trace CO) and no other C-containing by-products are detected. This high selectivity for CO_2 and trace CO has been observed on V-based catalysts [7]. The Cl balance reaches 80–85%, implying that deposition of Cl species on the surface of catalysts occurs. XPS analyses indicate that on the surface of the used catalysts there exists 1.5–4.5% Cl atom estimated from the peak of Cl 2p at 198.2–198.8 eV, ascribed to inorganic Cl species [50]. It is usually impossible to avoid the formation of chlorinated by-products during the oxidative destruction of chlorinated organics, especially in the presence of supported noble metal catalysts, where substantial amount of polychlorinated benzene is formed during catalytic combustion of CB [37,38]. In this work, reaction products were trapped in CB for 10 h at ~10 °C and then the products were collected to be analysed by GC (the minimum level of its detection is $\leq 2 \times 10^{-11}$ g/s (n-C16)). Results indicate that byproducts like dichlorobenzene or trichlorobenzene were far below the detection level if they were formed during the CB catalytic oxidation.

3.4. Stability study

For the catalytic combustion of CVOCs, catalyst deactivation is still a hurdle in commercial applications. The experiments for stability were carried out by feeding the stream containing 1000 ppm CB and 10% O_2 at 350 °C at space velocity 15,000 h^{-1}. As shown in Fig. 6, stable activity over pure MnO_x catalysts calcined at different temperatures is observed without a substantial decrease in conversion, although Mn-650 and Mn-750 show fairly low activity due to sintering during calcination. Over the catalysts MnCe-550 and MnCeLa-550 and MnCeLa-650, conversion within 1000 min almost maintains 98% or even higher, while over the catalysts MnCe-650, MnCe-750 and MnCeLa-750, the drop of activity during the first 100 min was observed, but after that, conversion reaches stable at 71%, 37% and 64%, respectively. The analyses by GC–MS showed that all catalysts under study have more than 99.5% selectivity to

CO_2 and no other C-containing by-products are detected. Moreover, carbon balance reaches 99.5%. It seems reasonable that the deactivation of these catalysts can result mainly from Cl species deposition. For the two former catalysts, strong adsorption of Cl on CeO_2 active sites separated from $MnCeO_x$ solid solution can be anticipated. As observed by our previous researches, pure CeO_2 catalysts deactivated quickly due to the strong adsorption of HCl or Cl_2 produced from the decomposition of trichloroethylene to blockade the active sites [48]. For the latter catalyst, La species can interact with Cl species at 350 °C [51], probably resulting in the destruction of $LaMnO_3$ on the surface.

3.5. The effect of water

Because of water detected in the exhaust gas, it is one part of the work to investigate the effect of water on the activity of MnCeLa-550 catalyst for CB combustion. CB conversion at various temperatures at the space velocity of 15,000 h^{-1} over MnCeLa-550 was observed as reaction proceeded in the presence of water while changing the CB concentration from 1000 to 2500 ppm. Results show that T_{50} was classified as 184, 204, 217 and 226 °C with water presence and as 158, 179, 196 and 200 °C without water presence at CB concentration of 1000, 1500, 2000 and 2500 ppm, respectively. This phenomenon indicates that water can affect the CB combustion over MnCeLa-550 catalyst. The effect of water on the oxidation of chlorinated aromatics has been studied on some occasions. Amiridis [52] found that water promoted at low temperature through the removal of Cl species and C species on the surface, but it inhibited at high temperature the oxidation of dichlorobenzene over V_2O_5/TiO_2 catalysts due to the adsorption of water on the active sites. Bertinchamps et al. [53] observed that the addition of water decreased the number of strong Brönsted acid sites involved in the adsorption of the chlorobenzene. On the other hand, the positive effect of water can promote the removal of surface chloride species in the form of HCl and thus favors the selectivity for carbon oxides formation by decreasing the amount of chlorinated by-products [54]. Therefore, water influences the reaction in a complicated way. Here, water inhibits CB combustion probably through its competition with reactant molecules for active sites. This inhibition was observed during the combustion of trichloroethylene over cerium oxide in wet air [48]. A possible explanation is that water is dissociated on the surface of CeO_2 into H^+ and OH^- species so as to retard the adsorption of oxygen molecules.

3.6. Kinetics consideration

The effect of inlet CB concentration on the reaction rate was investigated when reaction proceeded at the space velocity of 15,000 h^{-1} at 160 °C. Fig. 7 shows that reaction rate varies in different manners with the increase in the inlet CB concentrations from 500 to 2500 ppm. For MnCe-550, dependence of reaction rate on concentration is of first order within the range from 500 to 2000 ppm of CB. However, from 2000 up to 2500 ppm of CB concentration, the rate decreases, probably due to the deposition of more Cl species produced during the decomposition of CB [55]. For MnCeLa-550, dependence of rate on CB concentration could be described well by zero-order kinetics except for the situation at 500 ppm of CB. Hence, CB adsorption on the surface of MnCeLa-550 at 160 °C must not be rate limiting. The observed zero-order kinetics suggests that the catalyst surface is saturated by the reacting species within the overall reaction time. The reaction is probably limited by one of the processes on the surface that follows adsorption, e.g., reaction with oxygen species and desorption of products, such as Cl species, which has an inhibition effect on the reaction [48,56,57]. In this context, the experiments over MnCeLa-550 were carried out with raising O_2 concentration from 10% up to 20%,

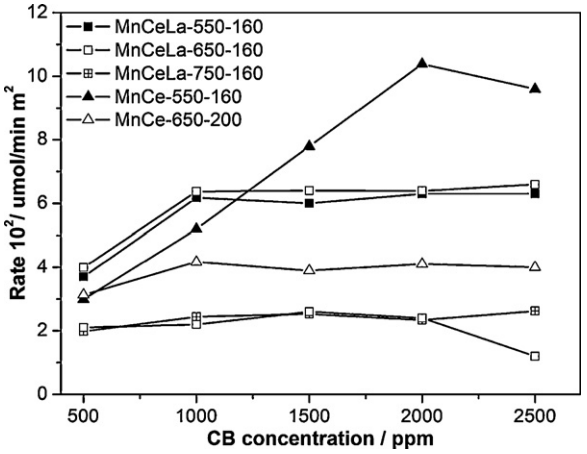

Fig. 7. The reaction rate at different CB concentration over MnCe and MnCeLa catalysts calcined at different temperature; –160, reaction at 160 °C; –200, reaction at 200 °C gas composition: 10% O_2, N_2 balance; GHSV = 15,000 h^{-1}.

maintaining 2500 ppm CB in feed. The results show that no difference in rate is found. Characterization of the used MnCeLa-550 by XPS confirmed that Cl $2p_{3/2}$ level is 198.5 eV, higher than that of the used MnCe-550 (198.2 eV), indicating that stronger adsorption of Cl species occurred. Substitution of La for part of Ce causes decrease in the amount of $MnCeO_x$ solid solution, and therefore, mobility of active oxygen reduces. Higher activity of MnCeLa-550 shown in Fig. 5 is ascribed to higher surface area, which means more active sites are available. The reaction at 200 °C (while other reaction conditions remain the same) but becomes zero order in kinetics over MnCe-650. After reaction, this catalyst shows Cl $2p_{3/2}$ level at 198.8 eV. In the case of MnCeLa-650, the reaction rates at different CB concentrations keep almost as same as that over MnCeLa-550, and shows zero-order in kinetics. Moreover, Cl $2p_{3/2}$ peak appears at 198.4 eV. From these data, it can be concluded that kinetics in CB combustion over catalysts under study is correlated to the strength of adsorption of Cl species. In other words, the stronger the Cl adsorbs, the lower the activity of the catalysts is observed.

3.7. Comparison with benzene combustion

In order to further understand CB combustion over Mn based catalysts, the catalytic combustion of chlorine-free molecule benzene was investigated. It can be seen in Fig. 8 that T_{50} of benzene

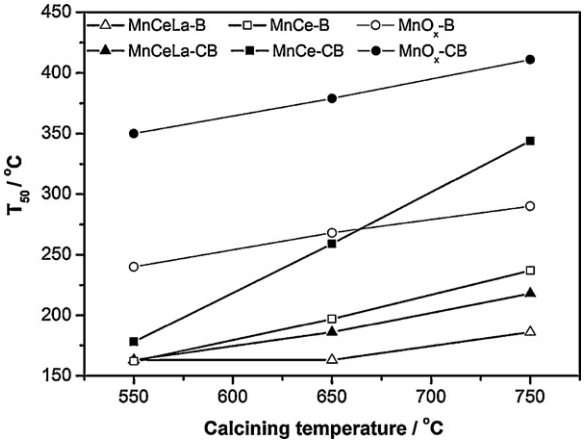

Fig. 8. Comparison between activities for CB and benzene combustion over MnCe and MnCeLa catalysts caicined at different temperature; -B, for benzene; -CB, for chlorobenzene; gas composition: 1000 ppm CB, 10% O_2, N_2 balance; GHSV = 15,000 h^{-1}.

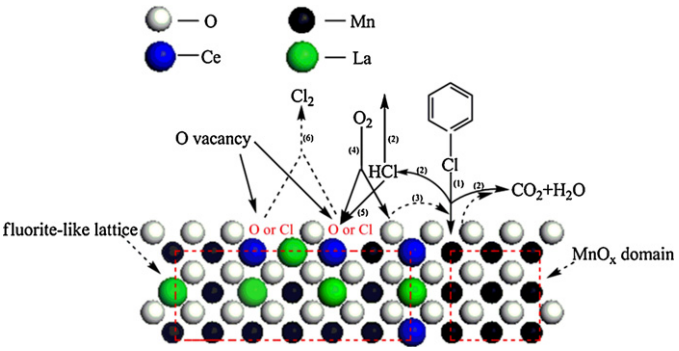

Scheme 1. Plausible Mechanism for CB Combustion on MnCeLa Catalyst.

combustion increases with the increase in calcining temperature. For pure MnO_x catalysts, T_{50} increases from 240 °C on Mn-550 to 290 °C on Mn-750. However, T_{50} of CB combustion on the corresponding MnO_x catalysts is much higher, 350 °C for Mn-550 and 420 °C for Mn-750. In the case of MnCe catalysts, T_{50} for benzene combustion is low, although it increases gradually with the increase of calcining temperature. This phenomenon indicates that MnCe catalysts are highly active. Conversely, T_{50} of CB combustion on MnCe-750 increases by 110 °C, in comparison to that on MnCe-550. It is interesting to find that the difference of T_{50} between benzene and CB conversion on MnCeLa catalysts calcined at different temperature is small, even for MnCeLa-750 catalyst. And the same phenomenon occurs on MnCe-550. Considering the fact that MnCe-550, MnCeLa-550 and MnCeLa-650 with more oxygen species present high activity, it can be seen that the amount of active oxygen is critical to the oxidation of CB and benzene. For the oxidation of CB, the increase of active oxygen species can weaken the adsorption of Cl species. Over MnCeLa-550 and MnCe-550, there is much amount of oxygen species to promote the removal Cl species. With raising calcining temperature, the interface area between MnO_x and $MnCeO_x$ will decrease due to sintering or the isolation of MnO_x from $MnCeO_x$ for MnCe catalysts, thus, leading to the decrease in the amount of active oxygen species. For the oxidation of benzene, this change in interface area will not affect the reaction so much as the CB combustion, because no removal of Cl species is involved. The removal of Cl species from the surface is dependent on the oxygen species while the adsorption of Cl species inhibits the dissociation of oxygen molecules. Therefore, the difference in combustion activity between CB and benzene will increase with the decrease in mobility of oxygen. Compared with MnCe-550, catalysts MnCe-650 and MnCe-750 present poor mobility of oxygen, due to the isolation of Mn species from $MnCeO_x$, and therefore the removal of Cl species becomes slow. For pure MnO_x catalysts calcined at various temperatures, mobility of oxygen is poorer and therefore, the activity for CB combustion is, as expected, much lower than that for benzene combustion. High stability of MnCeLa catalysts maintains the interface of MnO_x and $MnCeO_x$ solid solution so that the removal of Cl species becomes smooth.

In order to obtain deep insights into this reaction, a mechanism consisting of six elementary steps is schematized (Scheme 1): (1) absorption of CB on the active Mn species (interface between MnO_x and $MnCeO_x$ is where the most activity sites lie) and their neighbor lattice O; (2) reaction of adsorbed CB species with the lattice O from MnO_x to produce CO_2, H_2O and HCl; (3) migration of the lattice/adsorbed O from CeO_2 grains to MnO_x domains to replenish the consumed oxygen; (4) adsorption of the gas-phase oxygen on the surface of CeO_2 grains probably around the O vacancies; (5) a small part of the produced HCl back to the surface of catalyst, and absorbed on the O vacancies or some active sites for the transformation of oxygen; and (6) promotion of removal of Cl species by the active oxygen species, and desorption of the absorbed Cl species from the catalyst surface in the formation of Cl_2. Obviously, the mobility of oxygen becomes dominant for the combustion of CB as well as for the removal of Cl.

Obviously, the mobility of oxygen and the interface between MnO_x and $MnCeO_x$ are the critical factors for CB combustion. In particular, the mobility of oxygen becomes dominant for the combustion of CB as well as for the removal of Cl. With the addition of Ce species, the $MnCeO_x$ solid solution is formed. It makes the O atoms in the catalysts locating in a perturbed chemical surrounding, which leads to highly mobility of oxygen during the reaction. The interface between MnO_x and $MnCeO_x$ is where the most active sites lie, and changes in the local surrounding, caused through the calcination at high temperature may destroy these active sites. However, the addition of La species into MnCe catalysts improves thermal stability of the catalysts, thus the interface between MnO_x and $MnCeO_x$ is stable even at high calcinations temperature.

4. Conclusion

Mn-based mixed-oxide catalysts modified with Ce and La were prepared by the method to form complexes and tested in the catalytic combustion of CB. The addition of Ce can cause the formation of $MnCeO_x$ solid solution with fluorite structure, while La can promote the dispersion of $MnCeO_x$ and MnO_x, as well as the stability of $MnCeO_x$. High mobility of oxygen on the interface between $MnCeO_x$ and MnO_x is critical to remove Cl species produced during CB decomposition. The deactivation of MnCe catalysts calcined at high temperature is ascribed to the isolation of MnO_x from $MnCeO_x$ solid solution as well as the enrichment in CeO_2 on the surface. MnCeLa catalysts, because of high activity of CB combustion and high thermal stability, become useful in the practice of removal of chlorinated aromatics.

Acknowledgements

We would like to acknowledge the financial support from National Basic Research Program of China (no. 2010CB732300, 2011AA03A406) and National Natural Science Foundation of China (no. 20977029).

References

[1] M.J. Morra, V. Borek, J. Koolpe, J. Environ. Qual. 29 (2000) 706–715.
[2] F. Alonso, I.P. Beletskaya, M. Yus, Chem. Rev. 102 (2002) 4009–4091.
[3] M. Taralunga, B. Innocent, J. Mijoin, P. Magnoux, Appl. Catal. B: Environ. 75 (2007) 139–146.
[4] F. Bertinchamps, C. Gregoire, E.M. Gaigneaux, Appl. Catal. B: Environ. 66 (2006) 1–9.
[5] M. Taralunga, J. Mijoin, P. Magnoux, Catal. Commun. 7 (2006) 115–121.
[6] F. Bertinchamps, M. Treinen, P. Eloy, A.M. Dos Santos, M.M. Mestdagh, E.M. Gaigneaux, Appl. Catal. B: Environ. 70 (2007) 360–369.
[7] F. Bertinchamps, C. Gregoire, E.M. Gaigneaux, Appl. Catal. B: Environ. 66 (2006) 10–22.
[8] F. Bertinchamps, C. Poleunis, C. Grégoire, P. Eloy, P. Bertrand, E.M. Gaigneaux, Surf. Interface Anal. 40 (2008) 231–236.
[9] A.H. Reidies, Ullmann's Encyclopedia of Industrial Chemistry, vol. A16, VCH, Weinheim, 1990, p. 123.
[10] M. Baldi, E. Finocchio, G. Busca, Appl. Catal. B: Environ. 16 (1998) 43–51.
[11] M. Baldi, V.S. Escribano, J.M.G. Amores, F. Milella, G. Busca, Appl. Catal. B: Environ. 17 (1998) 175–182.
[12] C. Lahousse, A. Bernier, P. Grange, B. Delmon, P. Papaefthimiou, T. Ioannides, X.V. Kios, J. Catal. 178 (1998) 214–225.
[13] V.P. Santos, M.F.R. Pereira, J.J.M. órfão, J.L. Figueiredo, Appl. Catal. B: Environ. 99 (2010) 353–363.
[14] Sang Chai Kima, Wang Geun Shim, Appl. Catal. B: Environ. 98 (2010) 180–185.
[15] C.N. Costa, V.N. Stathopoulos, V.C. Belessi, A.M. Efstathiou, J. Catal. 197 (2001) 350–364.
[16] X.Y. Wang, Q. Kang, D. Li, Appl. Catal. B: Environ. 86 (2009) 166–175.
[17] X.Y. Wang, Q. Kang, D. Li, Catal. Commun. 9 (2008) 2158–2162.
[18] M. van den Bossche, S. McIntosh, J. Catal. 255 (2008) 313–323.

[19] A. Machocki, T. Ioannides, B. Stasinska, W. Gac, G. Avgouropoulos, D. Delimaris, W. Grzegorczyk, S. Pasieczna, J. Catal. 227 (2004) 282–296.
[20] B. Zhang, D. Li, X.Y. Wang, Catal. Today 158 (2010) 348–353.
[21] M.F. Wilkes, P. Hayden, A.K. Bhattacharya, Appl. Surf. Sci. 206 (2003) 12–19.
[22] X.Y. Chen, Y. Liu, G. Niu, Z.X. Yang, M.Y. Bian, A.D. He, Appl. Catal. A: Gen. 205 (2001) 159–172.
[23] J.R. González-Velasco, A. Aranzabal, R. López-Fonseca, R. Ferret, J.A. González-Marcos, Appl. Catal. B: Environ. 24 (2000) 33–43.
[24] R. López-Fonseca, A. Aranzabal, J.I. Gutiérrez-Ortiz, J.I. Álvarez-Uriarte, J.R. González-Velasco, Appl. Catal. B: Environ. 30 (2001) 303–313.
[25] L. Dimesso, L. Heider, H. Hahn, Solid State Ionics 123 (1999) 39–46.
[26] M. Machida, M. Uto, D. Kurogi, T. Kijima, Chem. Mater. 12 (2000) 3158–3164.
[27] Q. Ye, B.Q. Xu, Acta Phys. Chim. Sin. 22 (2006) 345–349.
[28] M.F. Wilkes, P. Hayden, A.K. Bhattacharya, J. Catal. 219 (2003) 286–294.
[29] S. Ponce, M.A. Pena, J.L.G. Fierro, Appl. Catal. B 24 (2000) 193–205.
[30] Y. Ng Lee, R.M. Lago, J.L. Fierro, V. Cortes, F. Sapina, E. Marinez, Appl. Catal. A 207 (2001) 17–24.
[31] M. O'Connell, A.K. Norman, C.F. Hüttermann, M.A. Morris, Catal. Today 47 (1999) 123–132.
[32] Y. Zhang-Steenwinkel, J. Beckers, A. Bliek, Appl. Catal. A 235 (2002) 79–92.
[33] Y. Ng Lee, R.M. Lago, J.L.G. Fierro, J. González, Appl. Catal. A 215 (2001) 245–256.
[34] Z. Yu, L. Gao, S. Yuan, Y. Wu, J. Chem. Soc. Faraday Trans. 88 (1992) 3245–3249.
[35] E. López-Navarrete, A. Caballero, A.R. González-Elipe, M. Ocaña, J. Eur. Ceram. Soc. 24 (2004) 3057–3062.
[36] F. Kapteijn, L. Singoredjo, A. Andreini, Appl. Catal. B: Environ. 3 (1994) 173–189.
[37] J. Carnö, M. Ferrandon, E. Björnbom, S. Järås, Appl. Catal. A: Gen. 155 (1997) 265–281.
[38] J. Trawczyński, B. Bielak, W. Miśta, Appl. Catal. B: Environ. 55 (2004) 277–285.
[39] F. Arena, G. Trunfio, J. Negro, B. Fazio, L. Spadaro, Chem. Mater. 19 (2007) 2269–2276.
[40] A. Nineshige, T. Taji, Y. Muroi, M. Kobune, S. Fujii, N. Nishi, M. Inaba, Z. Ogumi, Solid State Ionics 135 (2000) 481–485.
[41] L.N. Ikryannikova, A.A. Aksenov, G.L. Markayan, G.P. Muravieva, B.G. Kostyuk, A.N. Kharlanov, E.V. Linina, Appl. Catal. A: Gen. 210 (2001) 225–235.
[42] M. Fernandez-García, A. Martínez-Arias, A. Iglesias-Juez, C. Belver, A.B. Hungría, J.C. Conesa, J. Soria, J. Catal. 194 (2000) 385–392.
[43] J.R. McBride, K.C. Hass, B.D. Poindexter, W.H. Weber, J. Appl. Phys. 76 (1994) 2435–2441.
[44] Y.F. Han, L. Chen, K. Ramesh, E. Widjaja, S. Chilukoti, I.K. Surjami, J.S. Chen, J. Catal. 253 (2008) 261–268.
[45] Y. Liu, Z. Wei, Z. Feng, M. Luo, P. Yang, C. Li, J. Catal. 202 (2001) 200–204.
[46] Y. Liu, M. Luo, Z. Wei, Q. Xin, P. Yang, C. Li, Appl. Catal. B: Environ. 29 (2001) 61–67.
[47] A.J. Zarur, J.Y. Ying, Nature 403 (2000) 65–67.
[48] Q.G. Dai, X.Y. Wang, G.Z. Lu, Appl. Catal. B: Environ. 81 (2008) 192–202.
[49] Y. Dai, X.Y. Wang, D. Li, Q.G. Dai, J. Hazard. Mater. 188 (2011) 132–139.
[50] M.A. Àlvarez-Montero, L.M. Gómez-Sainero, M. Martín-Martínez, F. Heras, J.J. Rodriguez, Appl. Catal. B: Environ. 96 (2010) 148–156.
[51] P. Van der Avert, B.M. Weckhuysen, Angew. Chem. Int. Ed. 41 (2002) 4730–4732.
[52] C.E. Hetrick, F. Patcas, M.D. Amiridis, Appl. Catal. B: Environ. 101 (2011) 622–628.
[53] F. Bertinchamps, A. Attianese, M.M. Mestdagh, E.M. Gaigneaux, Catal. Today 112 (2006) 165–168.
[54] G. Sinquin, C. Petit, S. Libs, J.P. Hindermann, A. Kiennemann, Appl. Catal. B: Environ. 32 (2001) 37–47.
[55] I.M. Freidel, A.C. Frost, K.J. Herbert, F.S. Meyer, J.C. Summers, Catal. Today 17 (1993) 367.
[56] R.W. van den brink, R. Louw, P. Mulder, Appl. Catal. B: Environ. 25 (2000) 229.
[57] R.W. van den brink, R. Louw, P. Mulder, Appl. Catal. B: Environ. 16 (1998) 219.